Final Draft
of the original manuscript:

Daneshpour, S.; Kocak, M.; Langlade, S.; Horstmann, M.:
Effect of overload on fatigue crack retardation of aerospace Al-alloy laser welds using crack-tip plasticity analysis
In: International Journal of Fatigue (2009) Elsevier

DOI: 10.1016/j.ijfatigue.2009.04.005

Effect of overload on fatigue crack retardation of aerospace Al-alloy laser welds using crack-tip plasticity analysis

S. Daneshpour*, M. Koçak , S. Langlade, M. Horstmann

GKSS Research Centre, Institute of Materials Research,

D – 21502 Geesthacht, Germany

**Corresponding author.* E-mail: shahrokh.daneshpour@gkss.de

Abstract

Investigations on fatigue crack growth retardation due to single tensile and periodic multiple over load in strength undermatched laser beam welded 3.2 mm thick aerospace grade aluminium alloy 2139T8 sheets are conducted. The effect of overload on the fatigue crack propagation behaviours of the homogenous base metal and welded panels (200 mm wide, centre cracked) was compared using experimental and FE analysis methods. The effective crack tip plasticity has been determined in homogeneous M(T) specimens using Irwin's method and in both homogeneous and laser welded specimen by calculating crack tip plastic strain using FE analysis for single tensile overload. The crack retardation due to the overload in welded specimens are described by the Wheeler Model. The crack tip plastic zone size in the welded specimen was determined by FE analysis using maximum plastic zone extension at the mid sheet thickness. The results show that the Wheeler Model can be implemented to the highly heterogeneous undermatched weld to describe the crack retardation in fatigue following single tensile overload. Fatigue crack growth retardation due to single overload is found to be larger than the base metal. However, after periodic multiple overload, shorter crack retardation has occurred for undermatched welds than the base metal.

Keywords: Overloads, Fatigue crack growth, Plastic zone, Welded joints, Aluminium alloys.

1. Introduction

Laser beam welding (LBW) is already being used in several aircraft structures to reduce weight and fabrication cost by replacing the conventional riveting technology. By use of the LBW technology, it is currently practised to fabricate integral stiffened panels containing T-joints between stringer and skin sheet. This advanced LBW technology is capable to produce highly complex and competitive airframe parts for current and future metallic aircrafts. Some parts of the aircraft structure require more stringent damage tolerance consideration than other parts due to different loading conditions. For example, upper fuselage parts operate generally under tension while bottom parts under compression and hence both require different design rules and material performance. Currently, considerable amount of LBW panels are used in lower fuselage sections of some civil aircrafts. However, in order to extend the current application area of the welded panels, it is essential to improve current level of knowledge on the damage tolerance performance of the welded Al-alloy components. As all aircraft structures are subjected to cyclic loading during their service life, fatigue crack initiation and propagation are two main areas of interest to improve structural performance of the aircrafts. Knowingly, damage tolerance design concept is based on the initial flaw and hence fatigue crack propagation (FCP) performance becomes paramount importance to describe design life and inspection intervals.

Aircraft structure operates under spectrum load fatigue (cyclic loading with variable stress amplitude) where load history effects occur. The occurrence of positive overloads or high-low load sequence, for example, has strong effect on the crack propagation behaviour while these lead to favourable crack growth retardation.

A number of equations have been developed to describe the fatigue crack propagation behaviour (da/dN - ΔK relationship).The well-known Paris&Erdogan [1] describes the FCP behaviour in a most principal fashion and further models contain parts to include various effects which play important role to describe the FCP behaviour. It should be noted that the FCP behaviours and their predictions performed under constant amplitude loading differ considerably

from variable amplitude loading conditions where latter should include load interaction effect. It is known that the application of a single overload (OL) cause a decrease in the crack growth rate (retardation, delay of the crack growth) [2-6]. This retardation remains in effect for a period of loading after the overload while crack has to overcome a larger plastic zone size (i.e. higher crack closure) occurred at the incident of the OL. The crack growth retardation increases exponentially with the increase of the overload ratio (OLR*)*, which describes the magnitude of the overload over the maximum load in the constant amplitude loading. Full crack arrest may occur in high OL ratios [7].

The delay phenomenon of fatigue crack growth followed after a tensile overload (compressive over load – under load- generally causes an acceleration in the crack growth rate) can be explained mainly by compressive residual stresses ahead of the crack tip and crack closure (induced by plasticity). Having lower strength property in the weld zone, confined plastic zone development within the weld may occur where the size and shape differ significantly than the crack in the homogeneous materials. In turn, this affects the retardation behaviour of the crack at the vicinity of the weld. The period of crack growth retardation is longer for materials that develop larger plastic zone sizes, such as low yield strength materials, zones or thin sections. The yield strength of laser beam welds of Al-alloys can significantly be lower than the base metal. In this context, it is important to describe the crack growth retardation phenomena for the weld regions of Al-alloys where strong property gradient usually exist within a narrow zone. Currently, lack of knowledge exists in this field and hence present study aims to address to this issue.

Crack Retardation Models

Numbers of models have been developed to describe the fatigue crack growth behaviour after applying OL for homogeneous materials [8-15], but no model exists for description of crack retardation event in welds. Here some of the models will briefly be described.

Elber [9] employed the crack closure concept to explain the crack growth retardation after applying OL. With respect to the constant amplitude loading, the OL caused large compressive

stresses at the crack tip resulting in crack closure. A large portion of the subsequent tensile load had to be used to ‘‘open’’ the crack, leading to a much smaller ‘‘effective’’ load and the crack growth retardation. Here, it should also be added that when underload follows an overload reduces the amount of crack growth retardation. The model of Matsuoka et al. [10] was also based on the crack closure concept, with a consideration of crack tip blunting. Wheeler [11] emphasized the enlarged plastic zone ahead of the crack tip caused by overloading. The crack tip must grow beyond the affected zone created by overloading before the crack growth rate can return to the stable values. Sheu et al. [13] defined the Wheeler retardation parameter as ‘‘a power function of the ratio of the present plastic zone size (i.e., diameter of the plastic zone) to the distance from the crack tip to the border of the plastic zone caused by the OL’’. Lui [14] provided a further explanation of this concept. Lu and Li [15] argued that several co-existing and mutually competitive mechanisms were involved in the fatigue crack growth after applying OL. In addition to crack closure and compressive residual stresses, other mechanisms such as crack tip blunting and strain hardening may accelerate the crack growth rate. In general, methods to predict fatigue crack growth under variable amplitude loading can be grouped into three basic categories namely; crack closure models, statistical models and crack tip plasticity models. All of these based on the linear elastic fracture mechanics concepts and attempted to take into account for load interaction effect (retardation).

The crack tip plasticity models assume that retardation occur mainly due to the large plastic zone developed during the OL. The favourable effect remains active as long as the plastic zones developed during the subsequent load cycles remain within the plastic zone of the OL. The well-known models in this category developed by Wheeler [11] and Willenborg [12]. From these two major crack tip plasticity models, Wheeler Model is described below and used to describe the retardation effect for laser weld zones in this study. It is intended to see the limits (if any) and applicability of the model and define further tasks to overcome the limits.

Wheeler Model [11] basically modifies the constant amplitude growth rate with an empirical retardation parameter of, C_p, and this can be added to the right side of the Paris law to consider load interaction effects as following:

$$\frac{da}{dN_i} = \left(C_p\right)_i \left[C\left(\Delta K_i\right)^m\right] \quad \text{(Eq. 1)}$$

It is clear that $C_p = 1$ is for constant amplitude loading and varies from 0 to 1. This model is widely used to consider the overloading effect due to its simplicity. In the Wheeler Model [11], this retardation parameter C_p is defined as a function of the ratio of the current plastic zone size to the plastic zone size produced by the incident of OL:

$$\left(C_p\right)_i = \left(\frac{r_{yi}}{a_p - a_i}\right)^p \quad \text{(Eq. 2)}$$

where a_i represents the current crack length at the i^{th} loading cycle, r_{yi}, denotes the current plastic zone size due to the i^{th} loading cycle, a_p is the sum of the crack length at which the OL was applied and the plastic zone created by the OL (Fig. 1), and p is the Wheeler empirically-adjustable shaping exponent which can be simply taken as the value that best fits the data. The empirical shaping exponent, p, must be determined experimentally and can not be determined in advance of testing.

According to this model, as mentioned above the crack growth delay will occur as long as the current plastic zone lies within the plastic zone created by the OL. As soon as the boundary of the current plastic zone reaches the boundary of the plastic zone created by the OL, the crack growth retardation will stop (i.e., $C_p = 1$). This model assumes that retardation proportionally decreases to the penetration of the crack tip into the plastic zone of the overload and does not take into account of the negative effect of compressive peak load on crack growth rate. Nevertheless, due to its principal suitability to the strength undermatched welds (where extensive plasticity occurs at the crack tip if it is placed at the vicinity of weld zone), this model was selected to apply to our case.

In the homogenous materials, the plastic zone size required in the Wheeler Model is often calculated by using Irwin's method [16]. On the crack plane, the plastic zone size under cyclic loading is estimated as [17]:

$$r_p = \frac{1}{\beta\pi}\left(\frac{\Delta K_I}{2Rp_{0.2}}\right)^2 \quad \text{(Eq. 3)}$$

While the monotonic OL plastic zone size is calculated as [1]:

$$r_p = \frac{1}{\beta\pi}\left(\frac{K_{SOL}}{Rp_{0.2}}\right)^2 \quad \text{(Eq. 4)}$$

In equations 3 and 4, β = 1 for plane stress and 3 for plane strain conditions. ΔK_I is the stress intensity factor range at the i^{th} loading cycle and K_{SOL} is the stress intensity factor corresponding to the single OL and $Rp_{0.2}$ is the yield stress of the material.

In this study, the thickness of specimens is 3.2 mm, so plane stress conditions are expected to prevail and therefore β = 1 is assumed to calculate the crack tip plastic zone size in homogeneous specimens.

Description of the crack retardation due to single over load (SOL) for welds is one part of the problem need to be evaluated. Application of periodic multiple tensile overloads (MOL) will increase the retardation effect, until a certain level of saturation. The placing of the spacing between each tensile overload is obviously critical and poses another variable. The effect of periodic tensile overload was also studied to compare homogeneous and welded specimens to establish the basic features of the MOL in undermatched welds.

Despite the extensive work on fatigue crack growth in the homogenous materials, there is still a need to develop and evaluate applicable methods to predict the fatigue crack propagation rate in the heterogeneous materials and later apply to the welded structures. In the current investigation, fatigue crack growth experiments and numerical simulation were conducted on homogeneous specimen and strength undermatched welds of Al 2139-T8. The effects of single and multiple tensile overloads on fatigue crack growth were studied. The Wheeler Model was evaluated critically

based on the experimental and numerical results of welded and homogeneous specimens. The experimental study has been done to obtain the crack growth rate and the material constant, *m* and *C* of the Paris law and *p* of the Wheeler Model. The numerical study has been performed to obtain the crack tip plastic zone size due to the SOL and the constant amplitude loading. The MOL case was not covered by the numerical analysis and only experimental results were presented. However, it is intended to extend current study to try to predict retardation due to MOL.

2. Experiments

The experimental fatigue crack propagation testing consisted of subjecting centre-cracked specimens to either single tensile or periodic multiple overloadings within constant amplitude fatigue loading. The fatigue crack growth tests were basically conducted in accordance with ASTM E 647 [18]. The test method covers the determination of fatigue crack growth rates from fatigue testing, including discussions on special requirements for various specimen configurations and recommended techniques for calculating the fatigue crack growth rates for homogeneous materials.

The material used in this study is Al 2139-T8 sheets with a thickness of 3.2 mm. The chemical composition and the mechanical properties of the aluminium alloys are presented in Table 1 and Table 2, respectively [19-21]. The test specimens used in the fatigue investigation were M(T) specimens with a centre-crack shown in Fig. 2. The specimens were cut lengthwise in the rolling direction of the aluminium alloy to be approximately 600 mm long, 200 mm wide and possessing a notch length ($2a_0$) of 7.0 mm in middle of specimen. The FZ width of welded specimens, $2H$, is 2.2 mm and the HAZ (Heat Affected Zone) size is 2.3 mm.

A 300 kN servo-hydraulic universal testing machine was used to perform the fatigue experiments. A travelling microscope consisting of a microscope at 10X magnification attached to two micrometers with resolutions of 0.01 mm was used to measure incremental fatigue crack growth. The fatigue loading on the specimens was comprised of axial tension in a sinusoidal wave form at room temperature in air. The baseline constant amplitude loading consisted of cycles at

maximum load of 80 MPa and stress ratio R (ratio of minimum stress, σ_{min}, to maximum stress, σ_{max}, as shown in Fig. 3) of 0.1 at a load frequency of 20 Hz. Single OL levels of 136 MPa were applied within the constant amplitude loading for the both single and multiple OL tests. The multiple overloading tests were conducted with periodic 1000 cycles between each OL application. In each test, the total crack length at which the first OL was applied, $2a_{sol}$, was approximately 20 mm.

Before the fatigue tests, each specimen was fatigue pre-cracked to a minimum length of 1.0 mm on both sides of the notch, as required by the standard, before valid crack length data was recorded. This procedure provides a sharpened fatigue crack of adequate size and straightness. The crack length data was calculated as an average of the left and right cracks, and then it was converted to the fatigue crack growth rate data using the secant and the incremental methods as recommended by the ASTM E 647 [18].

In order to define material constants of the Paris law, C and m, averaging of experimental crack length and corresponding number of cycles have been made according to ASTM E 647 [18], while the incremental average method was performed to define the Wheeler parameters. Here, specimen of Al 2139-T8 gives C = 7.4 x 10^{-7} and m = 2.32, where the crack growth rate is in *mm/cycle* and the stress intensity factor is in $MPa\sqrt{m}$.

3. Numerical Procedure

In order to evaluate the crack tip plastic zone needed in the Wheeler Model, FE analysis of an M(T) specimen was carried out. 3D FE simulation of the laser welded M(T) specimen with the dimensions identical to the specimens used in the experiments were conducted using ABAQUS. Elastic–plastic analysis and isotropic work hardening material characteristics have been chosen whereas the constitutive relations are given by Von Mises yield criterion. A M(T) specimen with a strength mismatched welded joint can be simply modelled as a tri-material system without considering residual stress and other types of non-linearity. Only a quarter of the M(T) specimen was analysed due to load and geometry symmetries.

Isotropic elasticity and plasticity are assumed for the weld zone (FZ), HAZ and BM. Table 1 presents the material properties used in the FE analysis [23-25]. With these values we can deduce the strength mismatch factor of M,

$$M = \frac{Rp_{0.2}^{FZ}}{Rp_{0.2}^{BM}} = 0.468 \quad \text{(Eq. 5)}$$

This low M-value indicates the plastic straining possibility of the fusion zone at a rather low crack tip loading level while base metal remains elastic and development of plastic zone may not penetrate into the base metal.

The element type used in the FE analysis is C3D8R (linear hexahedral with 8 nodes). In order to capture stress singularity in front of the crack tip, a fine mesh has been used to build the weld region and the area surrounding it. Several simulations were performed to estimate the effect of the mesh size on the result of the crack tip plasticity. The sizes of the finest elements are chosen between 0.1, 0.2, 0.35 and 0.5 mm to have at least 10 elements inside the monotonic crack tip plastic zone. The size of the elements in the weld region and its surroundings are 0.5 mm while the size of the elements selected in the remainder of the BM zone is 4.0 mm.

A preliminary simulation was performed to evaluate the effect of the HAZ on crack tip plasticity. The size of the plasticity obtained with a bi-material system (BM-FZ) appears to be 9 % lower than that of the tri-material system (BM-HAZ-FZ) whereas the resultant shape of the plastic zone in both models is similar. So in this study, the bi-material system has been chosen to analyse the fatigue behaviour of the welded specimens.

In order to simulate the development of the crack tip plasticity during the SOL, loads defined in Fig. 3 was applied to the edge of the M(T) specimen while the nodal displacements of another edge of the specimen are constrained by symmetrical condition. One stationary crack ($2a_{sol}$ = 20 mm) was defined inside the M(T) model. The crack tip plasticity is determined using plastic strain. In order to consider cyclic loading, the crack tip plastic zone sizes were calculated after applying an overload following with one cyclic loading and two constant cyclic loading as shown in Fig. 3.

In order to find the retardation parameter of the Wheeler Model, C_p, crack tip plastic zone size after applying SOL should be determined. The following steps were performed:

1. applying the SOL to define monotonic crack tip plastic zone
2. Dividing the resultant plastic zone due to the applied SOL into three zones with different yield stress surfaces. Each zone corresponds to the one third of the plasticity due to the OL, taking an average value of the corresponding yield stress.
3. Performing several simulations having a stationary crack at the beginning of each zone, $a_1 = a_{SOL} = 10mm$, $a_2 = a_{SOL} + a_{\min} + r_p^{SOL}/3$ and $a_3 = a_{SOL} + a_{\min} + 2r_p^{SOL}/3$, subjected to the load spectrum defined in Fig. 3. Here, $a_{\min}$ has defined the minimum crack length after applying SOL at which the minimum crack growth rate takes place and then crack growth dependence effect appears. $a_{\min}$ is taken as equal to one-quarter of the overload monotonic plastic zone size, r_p^{SOL}, as assumed by several authors[26]

4. Results and Discussions

Fig. 4a shows the experimental fatigue test results in terms of total crack length, 2a, vs. number of cycles for homogeneous and welded specimens under constant amplitude loading and SOL conditions. Fig. 4b is showing the periodic tensile over loads for base and weld metal panels including MOL results. In each condition, tests were repeated to increase the reliability to the data.

According to Fig. 4a, SOL extends fatigue life of the Al 2139-T8 base metal specimens about 5 %, while it increases the fatigue life of the welded panels approximately 80%. It is obvious that the final crack lengths that can be achieved in undermatched welds are shorter than the base metal (BM). It should be mentioned that these weld joints are made without any plate thickness increase (pad-up) which is usually utilised for such weld joints.

In comparing the fatigue life of BM and welded specimens, BM has a higher fatigue life than the welded specimen under the constant amplitude loading. But after applying SOL, the

welded specimens show higher fatigue life than the BM. In the other words, the effect of the SOL on fatigue life extension of the welded specimen is much higher than its effect on the BM whereas the effect of the MOL on fatigue life extension of the welded specimens is not as significant as its effect on the BM. Fig. 4b shows that MOL extends the fatigue life in BM approximately it around 480 %, while MOL increases the fatigue life for weld joint approximately 230 %.

Fig. 5 shows the experimental result of the crack tip plastic zones taken from the surface of the laser welded specimens subjected to SOL and MOL. Figures 5a and b are showing the specimen surfaces for SOL and MOL welded specimens respectively. The shapes of the crack tip plastic zones after applying SOL and 10 overloads (MOL) are also shown in Figure 5c and Figure 5d which are taken from surfaces of the same specimens using image analysis system ARAMIS. It is immediately obvious that the shape of the plastic zone development ahead of the crack tip is completely different from that of homogeneous material. In the undermatched welded specimen, overload induced plasticity is confined to the welded region and elongated in front of the crack tip. In the presence of cracks in the weld zone, plastic strain localization occurs at the crack tips even at nominally elastic applied loads, i.e. loads below the yield strength of the weakest material. Depending on the mismatch ratio, M, and width of the weld region the spread of the plastic zone can obtain different patterns in turn highly influences the crack tip loading as shown schematically in Fig. 6 [21]. The same applied load causes different plastic zone shapes and sizes ahead of the crack tip if width and local strength of the weld zone differs. For given applied load the crack driving force in the undermatched weld is higher than a crack would have in the base material.

It is apparent that the effects of SOL and periodic MOL on the fatigue crack propagation of base and weld metal specimens are different, Fig. 4. An improvement of fatigue life produced by SOL is much higher for the weld than the base metal due to much larger (extended) size of plastic zone development within the weld zone. However, an improvement after periodic MOL in undermatched weld zone is relatively modest again due to intensively confined plasticity evolution within narrow zone contrary to the base metal. This is an important observation and has

implications for the design of the components containing undermatched welds. In order to avoid elimination of the benefits of crack retardation, undermatched weld zones should be protected from intensely confined cyclic hardening. Fig. 5d is showing the plastic Mises strain distribution (after 10 overloads) which extends almost through entire specimen ligament.

Theoretically, a definition of the crack tip plastic zone size for such a heterogeneous sandwiched zones or weld cases is not available yet. A numerical model has been used to estimate the extension of the crack tip plastic zone size for this welded specimen. Fig. 7 is showing the shapes and distribution of the crack tip plastic zone development both in through thickness of the sheet and half surface of the weld. It is apparent that both FE analysis results, Fig. 7, and experimental results, Fig. 5a and Fig. 5c, yield similar shapes. It should be mentioned that in case of having coarse mesh, the FE results of the crack tip plasticity are strongly dependent on the mesh size. A good agreement between FE and experimental results of the crack tip plasticity size using havee been obtained for crack tip mesh sizes of smaller than 0.2 mm. According to Fig. 7 the maximum length of the crack tip plastic zone occurred in the mid-specimen thickness. In this study, this length has been taken as a plastic zone size needed in the Wheeler Model.

Fig. 8a shows the comparison of the experimental and predicted results of crack growth rate in homogenous M(T) specimen after applying constant cyclic loading and SOL. Here, predicting crack retardation after SOL has been performed by using the Wheeler Model (Eq. 1) where fitting parameter p = 0.2, determined by fitting the experimental data. In the comarision of Experimental and prediction results in Fig. 8a, the average size of retardation zone is almost equal to two times of size of the overload monotonic plastic zone. Here, a small retardation, in size and value, take places after SOL with decreasing of FCG within a zone which is almost equal to one-quarter of the overload monotonic plastic zone. Then FCG increases until the normal crack growth rate has reached where crack tip gets out of the plastic zone produced by SOL. Here, the size of the plastic zone after SOL (r_p^{SOL}) determined by Eq. 4 for base metal is found to be 1.31 mm. The Wheeler

Model can predict qualitatively the details of crack growth within the retardation zone due to single overload in homogeneous base metal.

In order to develop the Wheeler Model for the highly heterogeneous welded specimens, we need to define the material constants of the Paris law, the plastic zone size due to SOL and afterwards, as well as the fitting parameter, p, of the Wheeler Model. The same stress intensity factor and fitting method of the homogenous material were used for the welded specimen. The experimental and predicted results of welded specimens after applying constant amplitude cyclic loading and SOL are shown in Fig. 8b. According to Fig. 8b, after applying SOL, the crack growth rate decreased to its minimum value within a zone which is almost equal to one-quarter of the overload monotonic plastic zone. The crack growth rate recovered rapidly and then gradually approached the normal crack growth of constant amplitude loading. It is apparent that the transient zone size (which corresponds approximately to the range of 12.8 to 18 in terms of ΔK) is determined by the plastic zone caused by the overloading. Here, the size of the plastic zone after SOL (r_p^{SOL}) determined by FE analysis for the weld metal is found to be approximately 6.7 mm. The level of r_p^{SOL} for weld metal is much higher than the base metal (1.31 mm) which indicates that the WM will have much extensive crack retardation. The influence of the SOL, as expected diminished after the crack propagation out of the larger plastic zone created by the overload. According to the prediction line of the Paris law in Fig. 8b, $C = 2.6 \times 10^{-10}$ and $m = 5.7$ have been obtained for the welded specimen. Fig. 8b also shows predicted crack growth rate after applying SOL in the welded specimen by using Wheeler Model where $p = 0.5$ which is determined by fitting the experimental data related to the minimum crack growth rate after applying SOL. The estimated transient zone size has good agreement with the experimentally measured values. According to these results, the Wheeler Model can predict well the details of fatigue crack growth in the welded specimens through the retardation zone due to the SOL.

According to the Wheeler prediction lines in the welded and homogeneous specimens of Al 2139-T8 in Fig. 8a and Fig. 8b, the effect of the SOL on the crack retardation in the welded

specimen is higher than its effect in the homogeneous specimen. This is due to the fact that the size of the plastic zone occurring in the undermatched welded specimen is much larger (ΔK range of 5.2) than that occurring in the BM (ΔK range of ~2).

As Fig. 4b has revealed, effect of MOL on the crack retardation in welded specimen is not as significant as its effect in the BM. Other researchers' results show that when multiple tensile overloads are closely applied, they may interact with each other to either enhance or reduce the overall crack growth retardation. Such overload interaction is dependent on the relative magnitude and the spacing between overloads [22-28] or the frequencies of the overload application [29-33]. In other words, the overall crack growth retardation may be maximized by applying overloads at certain distances apart or at certain frequencies. At the same time, due to the aforementioned initial crack growth acceleration immediately following an overload, overloads that are applied too frequently can lead to lower overall crack growth retardation or even growth acceleration. It was also observed that crack growth retardation is reduced in the latter stage of fatigue life when the net section of the specimen approaches the yield strength of the material [34]. As observed in Fig. 5 and Fig. 7, the crack tip plastic zone of an undermatched welded specimen is confined to the weld area and elongated in front of the crack tip. It was observed that after applying the first OL, a longer plastic zone occurred in the welded zone when compared with that in BM. As a result in the welded specimen, the next OL occurred when the crack tip is inside the plastic zone caused by previous OL. Finally this condition leads to a reduction of the effect of MOL on crack retardation. In conclusion in the undermatched welded specimen, the trend is obvious from the test results (Fig. 4): a periodic overload in undermatched welded specimens with a 1000-cycle spacing between overloads is not as beneficial as in a homogeneous BM specimen.

Implementation of the Wheeler Model for the welded specimen has shown the same limitation as the application of this model for homogeneous specimens. The Wheeler Model can predict the tendency of the crack growth rate in the transient zone only after the minimum growth rate is reached. Major limitation of the Wheeler Model lies in the empirical nature of its shaping

exponent (p). This parameter bears no physical significance and is typically evaluated based on a trial-and-error approach to 'best fit' the experimental data. More importantly, the value of p in the Wheeler Model is not a material constant. Usually, p depends on the stress ratio, R, and the overload ratio, OLR [8]. As a result, the Wheeler Model has the potential for requiring a large database for the shaping exponents, each corresponding to a particular loading history. One remedy is to represent the Wheeler shaping exponent, p, as a function of R and OLR [8]. However, even for the same R and OLR, the value of p for the different crack length at which the overloading occurs can be different. Consequently, the Wheeler Model cannot predict the crack growth rate for a more general loading case.

To develop the Wheeler Model to the welded structures, there is still another limitation. Although the Wheeler Model takes the plastic deformation at the crack tip after overload into consideration, it is still mainly based on the stress intensity factor concept. The stress intensity factor reflects the elastic stress field near the crack tip and is only related to the external stress and the geometry of the specimen. However, the geometry of the weld is not considered, so the weld characteristics are handled by material constants, m and C. It is difficult for such a concept to consider the physical mechanisms governing the local plastic deformation and fracture at the crack tip located in the weld zone which is crucial for the crack growth. As a result, the parameters in the models lack physical meaning and can only are determined by fitting the crack growth experimental data.

5. Conclusions

In this study investigations on crack retardation due to the tensile over load in both laser welded and homogenous M(T) specimens of Al 2139-T8 are carried out by using experimental and FE methods. Features of fatigue crack growth retardation due to single and periodic multiple overloads were discussed. A mid-thickness extension of the crack tip plastic zone size of the welded specimen was used in the implementation of the Wheeler Model to the welded specimens. The following conclusions can be drawn from the current study:

1. Fatigue crack propagation tests of Al 2139-T8 and weld metal under constant amplitude loading revealed following Paris equation constants:

   Base Metal: $C = 7.4 \times 10^{-7}$ and $m = 2.32$

   Weld Metal: $C = 2.6 \times 10^{-10}$ and $m = 5.70$

2. In the undermatched welded specimen, the effect of the single overload on the retardation of the fatigue crack is found to be much effective, and leads to a higher fatigue life for the welded specimen than the BM. Crack tip plasticity induced by SOL determines the impact of overload on the retardation of FCG of undermatched welded specimens. This is due to the larger plastic zone size development in a confined surrounding by the higher strength base metal parts, $r_p^{WM} >> r_p^{BM}$.

3. Extensive occurrence of the plastic zone due to overload within undermatched weld region was analysed with 3D FE model with appropriate mesh size. The maximum crack tip mesh size was determined with the comparison of experimentally obtained plastic zone size. The plastic zone size at the mid-thickness was selected for Wheeler Model.

4. The Wheeler Model can predict the influence of the single overload on fatigue crack retardation in the undermatched welded specimen as well as the homogeneous specimen when an appropriate definition of the crack tip plastic zone size, specifically that it is confined to the weld region, is used. The shaping parameter, p, of the Wheeler Model is found to be for;

   Base Metal: $p = 0.2$

   Weld *Metal:* $p = 0.5$

6. Acknowledgements

The authors wish to thank Mr. S. Riekehr for his technical assistance in laser welding of specimens

7. References

[1] Rushton PA, Taheri F. Prdiction of crack growth in 350WT steel subjected to constant amplitude with over- and under-loads using a modified Wheeler approach. Marine Struct 2003; 16:517-39.

[2] McEvily AJ, Yang Z. The nature of the two opening levels following an overloading in fatigue crack growth. Metal Trans 1990; 21A (10):2717–27.

[3] Gan D, Weertman J. Fatigue crack closure after overload. Eng Fract Mech 1983;18(3):155–60.

[4] Schijve J, Broke D. The result of a test program based on a gust spectrum with variable amplitude loading. Aircraft Eng 1962; 34:314–6.

[5] Corbly DM, Packman PF. Influence of single- and multiple-peak overloads on fatigue crack propagation in 7075-T6511 Al. Eng Fract Mech 1973;5(2):479–97.

[6] Topper TH, Yu M T. The effect of overloads on threshold and crack closure. Int Jnl of Fatigue 1985;7(3):159–64.

[7] Nelson DV. Review of fatigue crack-growth prediction under irregular loading. Chicago, IL: Spring Meet, Society for Experimental Stress Analysis, 1975, pp. 11–6.

[8] Rushton PA, Taheri F. Prediction of crack growth in 350WTsteel subjected to constant amplitude with over- and under-loads using a modified Wheeler approach. Marine Struct 2003;16:517–39.

[9] Elber W. Fatigue crack closure under cyclic tension. Eng Fract Mech 1970; 2:37–45.

[10] Matsuoka S, Tanaka K, Kawahara M. The retardation phenomenon of fatigue crack growth in HT80 steel. Eng Fract Mech 1976;8: 507–23.

[11] Wheeler O. E. Spectrum loading and crack growth. J Basic Eng Trans ASME, Vol. D94, No 1, 1972, pp. 181–186.

[12] Willenborg, J, Engle RM, and Liu KW. A crack growth retardation model using an effective stress concept. AFFDL TM-71-1-FBR, Jan. 1971.

[13] Sheu BC, Song PS, Hwang S. Shaping exponent in Wheeler model under a single overload. Eng Fract Mech 1995;51(1):135–43.

[14] Lui AF. Structural life assessment methods. Materials Park, OH: ASM International; 1998.

[15] Lu Y, Li K. A new model for fatigue crack growth after a single overload. Eng Fract Mech 1993;46(5):49–856.

[16] Irwin GR. Analysis of stresses and strains near the end of a crack traversing a plate. Trans ASME J Appl Mech 1957;E24:361.

[17] Antunes FV, Borrego LFP, Costa JD, Ferreira JM. A numerical study of fatigue crack closure induced by plasticity. Fatigue Fract Eng Struct 2004;27:825–35.

[18] Standard test method for measurement of fatigue crack growth rates, ASTM E647-00, West Conshohocken (PA): American Society for Testing & Materials, 2000.

[19] Gérard H, Ehrström J.C, Cervi L, Eberl F. Towards fuselage panel friction stir welding. Aeromat 2005, Orlando USA, 06th-09th of June 05.

[20] WEL-AIR project, STREP 502 832. Development of Short Distance Welding Concepts for Airframes. Aeronautics Days 2006, Vienna Austria, 19-21 June 2006.

[21] Seib E. Residual strength analysis of laser beam and friction stir welded aluminium panels for aerospace applications. GKSS research center Geesthacht, Germany, 2006/3.

[22] Corbly DM, Packman PF. On the influence of single and multiple peak overloads on fatigue crack propagation in 7075-T6511 aluminium. Eng Fract Mech 1973;5:479–97.

[23] Mills WJ, Hertzberg RW. Load interaction effects on fatigue crack propagation in 2024-T3 aluminum alloy. Eng Fract Mech 1976;8:657–67.

[24] Cheng X, Okuhara Y, Yamada K, Kondo A. Fatigue crack growth rate measurement of structural steel under overload conditions. Proc JSCE, Struct Eng/Earthquake Eng 1994;11(1):45s–52s.

[25] Shuter DM, Geary W. Some aspect of fatigue crack growth retardation behaviour following tensile overloads in a structural steel. Fatigue Fract Eng Mater Struct 1996; 19(2/3):185–99.

[26] Lassen T., Recho N. Fatigue life analyses of welded structures ISTE Ltd, London,UK, 2006 pp.356-379.

[27] Hammouda MMI, Ahmad SSE, Seleem MH, Sallam HEM. Fatigue crack growth due to two successive single overloads. Fatigue Fract Eng Mater Struct 1998; 21:1537–47.

[28] Lang M, Marci G. The influence of single and multiple overloads on fatigue crack propagation. Fatigue Fract Eng Mater Struct 1999; 22:257–71.

[29] Vardar Ö, Yildirim N. Crack growth retardation due to intermittent overloads. Int J Fatigue 1990;12(4):283–7.

[30] Yildirim N, Vardar Ö. Study of periodic overloads at a fixed overload-ratio. Eng Fract Mech 1990;36(1):71–6.

[31] Tür YK, Vardar Ö. Periodic tensile overloads in 2024-T3 Al-alloy. Eng Fract Mech 1996;53(1):69–77.

[32] Skorupa M, Schijve J, Skorupa A, Zachwieja A. Experimental results and predictions on crack growth in a structural steel under periodically applied single and multiple overloads. In: Proceedings of the 17th international conference on offshore mechanics and arctic engineering, OMAE98-2453; 1998.

[33] Yamada K, Cao Q, Okuhara Y, Cheng X. Fatigue crack growth behaviour of various structural steel after single and periodic overloads. Proc JSCE, Struct Eng/Earthquake Eng 1998; 15(2): 191s–200s.

[34] Yuen B.K.C, Taheri F. Proposed modifications to the Wheeler retardation model for multiple overloading fatigue prediction. Int. J Fatigue 2006; 28:1803-1819.

Figures Captions

Fig. 1. Schematic view of plastic zone caused by overload and parameters used in Wheeler Model (Eq. 1 and Eq. 2) for base metal. The shape of the plastic zone will be distorted/extended for the weld metal crack

Fig. 2. Specimen layout and dimensions of a) base material M(T) specimen and b) laser welded M(T) specimen

Fig. 3. Cyclic load spectrum applied to the M(T) specimen during the experimental fatigue tests and FE analyses

Fig. 4. Experimental results of fatigue tests of welded and homogeneous specimens of Al 2139-T8; a) under constant amplitude loading and SOL, b) under constant amplitude loading, SOL and MOL

Fig. 5. Experimental results of the plastic zones due to a, c) SOL and b, d) MOL, taken from the surface of the welded specimen, shown confined plastic zone to the weld zone (soft zone)

Fig. 6. Plastic zone patterns for a) homogeneous material, b) undermatched welded specimen, $M = R_{P0.2W} / R_{P0.2B}$

Fig. 7. Numerical result of crack tip plastic zone caused by SOL, a view of through the thickness and on the face of half of the welded M (T) specimen

Fig. 8. Crack growth rates under constant amplitude loading and SOL in a) homogeneous M(T) specimen of Al 2139-T8 and b) the laser welded M(T) specimen of Al 2139-T8

Table 1. Nominal chemical composition of Al 2139-T8

Material	Si	Fe	Mg	Cu	Mn	Cr	Zn	Ti	Ag
Al 2139	0.1	0.15	0.25-0.8	4.5-5.5	0.2-0.6	0.05	0.25	0.1	0.3

Table 2. Tensile properties of Base Material, Heat Affected Zone and Fusion Zone of Al 2139-T8

	$R_{P0.2}$ (MPa)	R_m (MPa)	A (%)
Al 2139-T8	385	460	11.5
FZ	180	350	1.5

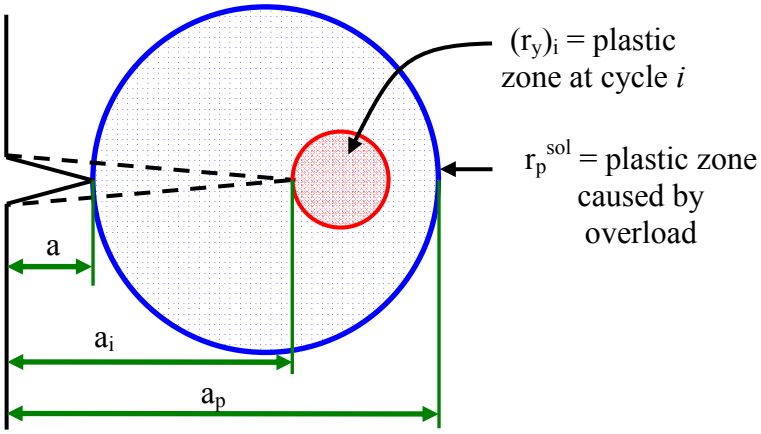

Fig. 5. Schematic view of plastic zone caused by overload and parameters used in Wheeler Model (Eq. 1 and Eq. 2) for base metal. The shape of the plastic zone will be distorted/extended for the weld metal crack

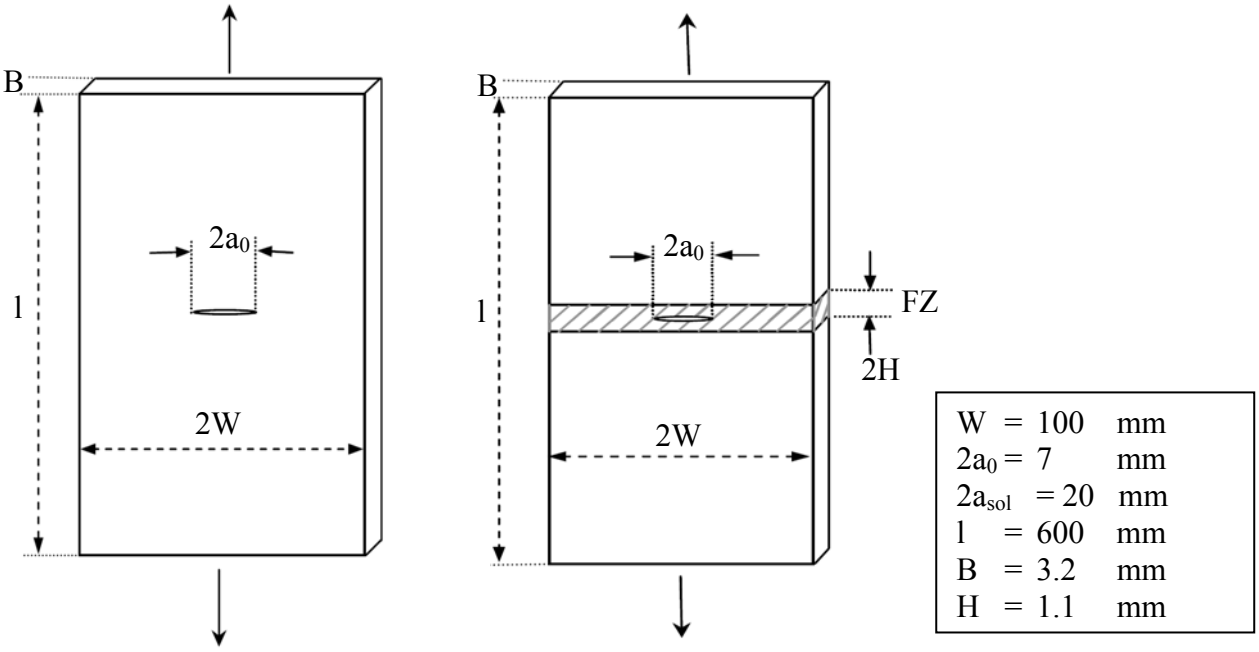

a) b)

Fig. 6. Specimen layout and dimensions of a) base material M(T) specimen and b) laser welded M(T) specimen

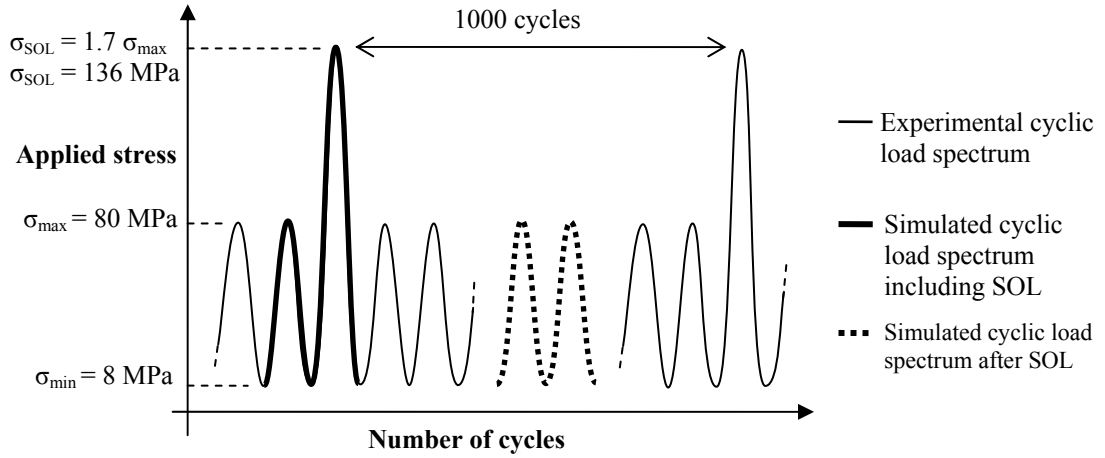

Fig. 7. Cyclic load spectrum applied to the M(T) specimen during the experimental fatigue tests and FE analyses

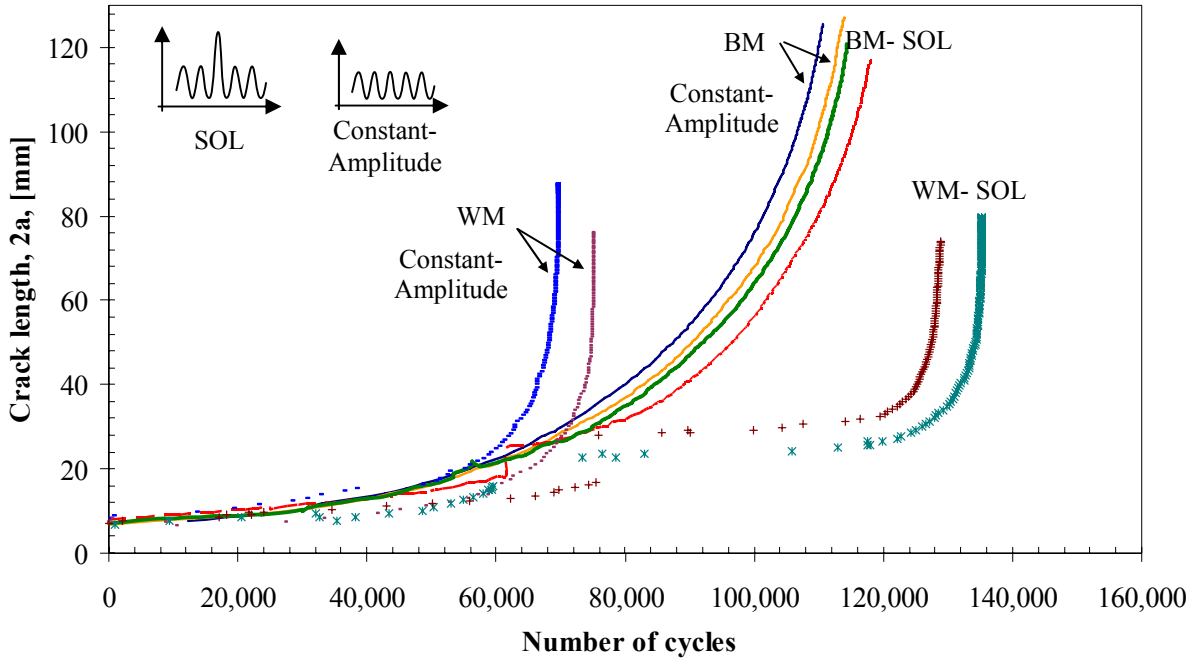

a)

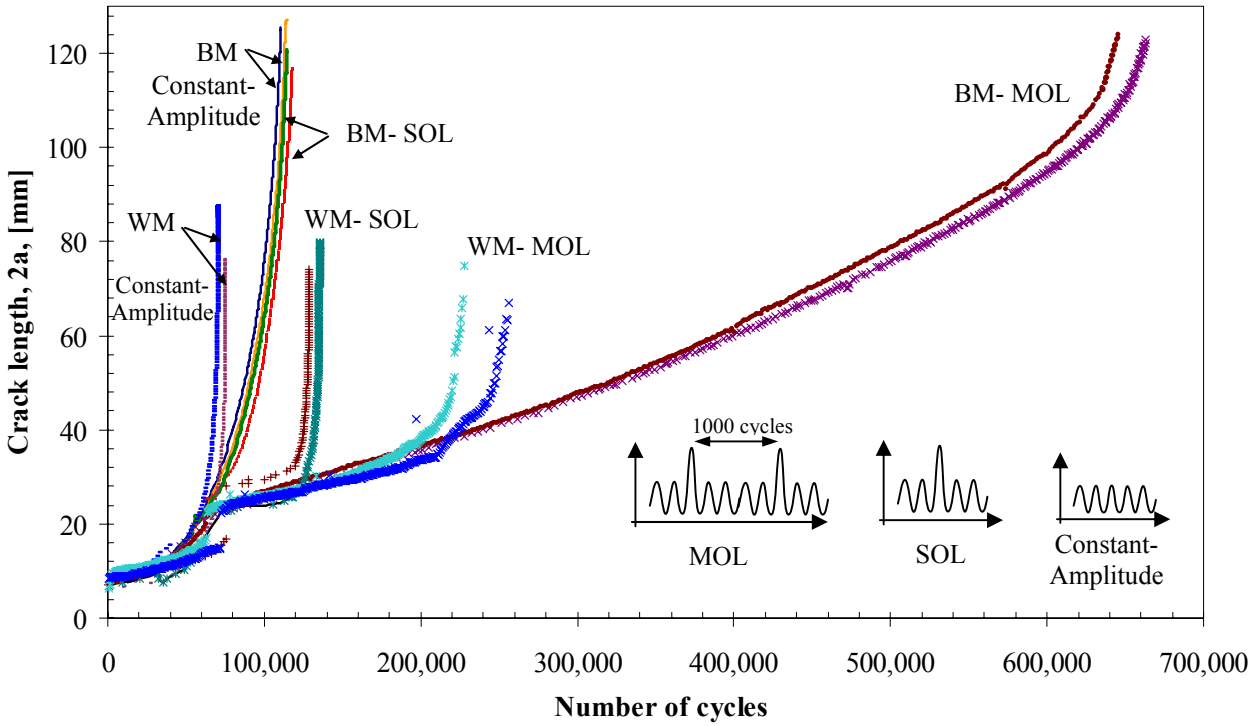

b)

Fig. 8. Experimental results of fatigue tests of welded and homogeneous specimens of Al 2139-T8; a) under constant amplitude loading and SOL, b) under constant amplitude loading, SOL and MOL

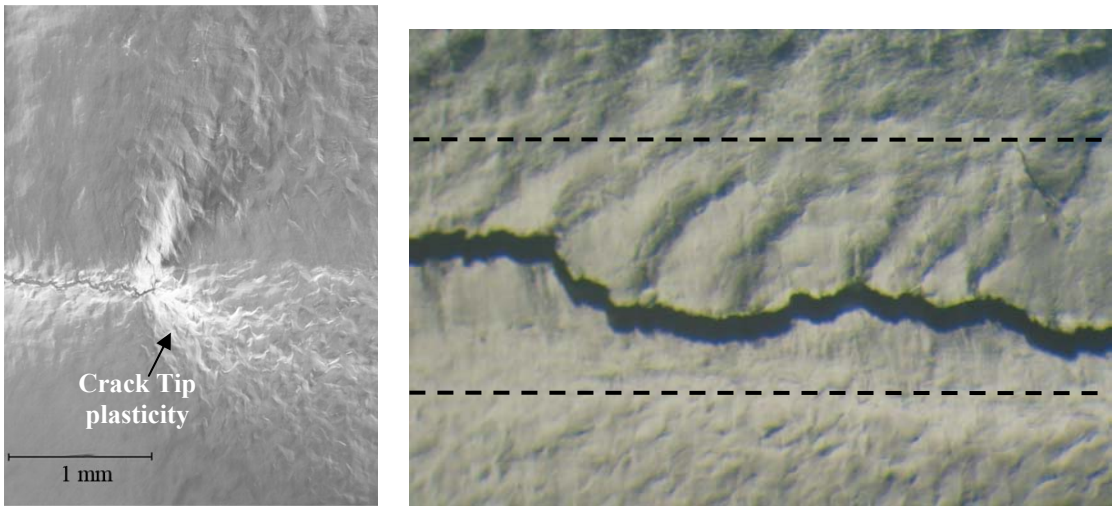

a) b)

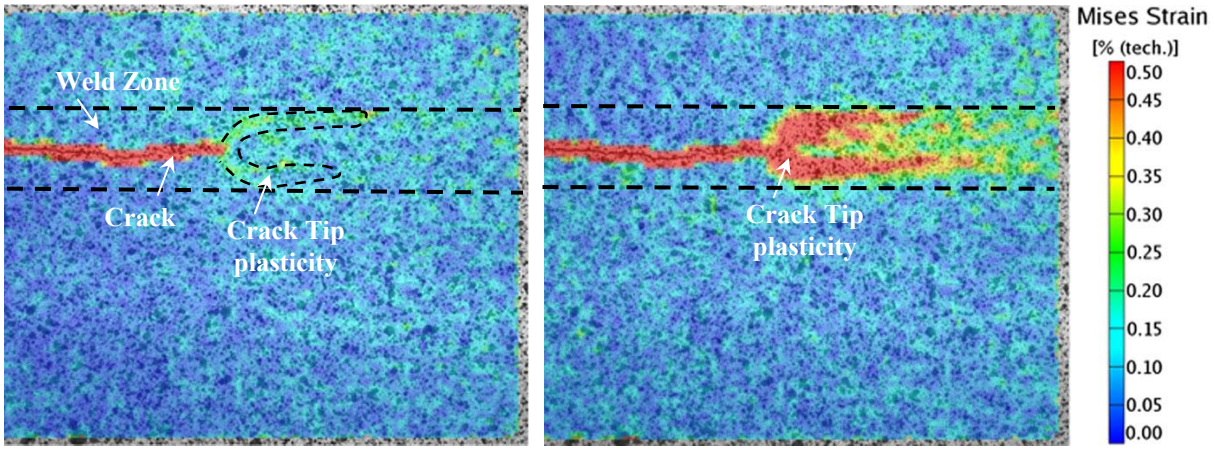

c) d)

Fig. 5. Experimental results of the plastic zones due to a, c) SOL and b, d) MOL, taken from the surface of the welded specimen, shown confined plastic zone to the weld zone (soft zone)

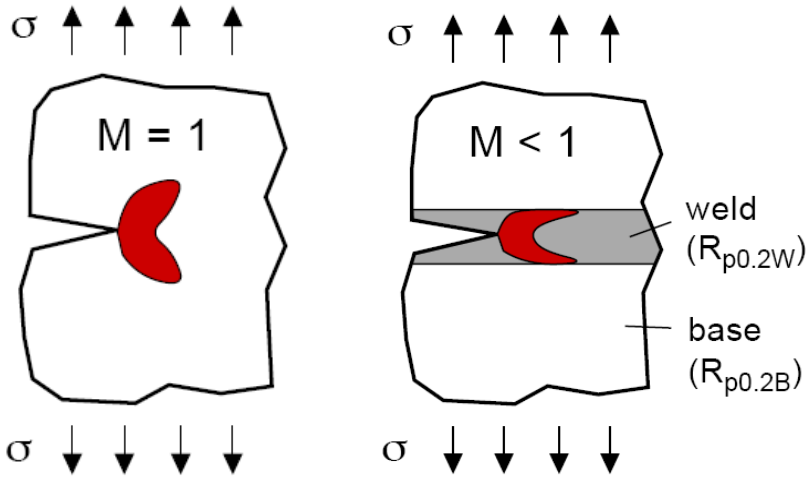

a) b)

Fig. 6. Plastic zone patterns for a) homogeneous material, b) undermatched welded specimen, $M = R_{P0.2W} / R_{P0.2B}$

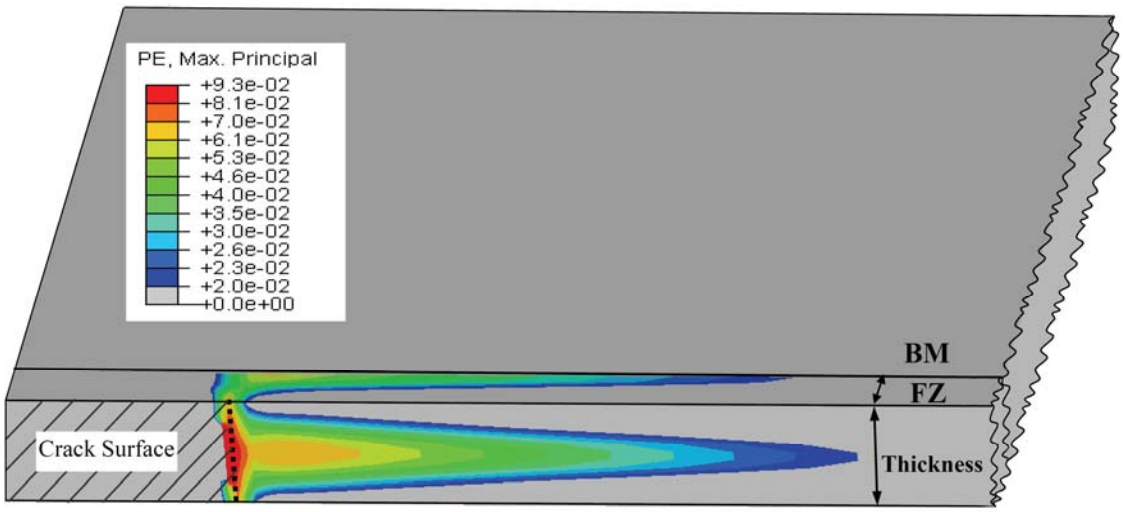

Fig. 7. Numerical result of crack tip plastic zone caused by SOL, a view of through the thickness and on the face of half of the welded M (T) specimen

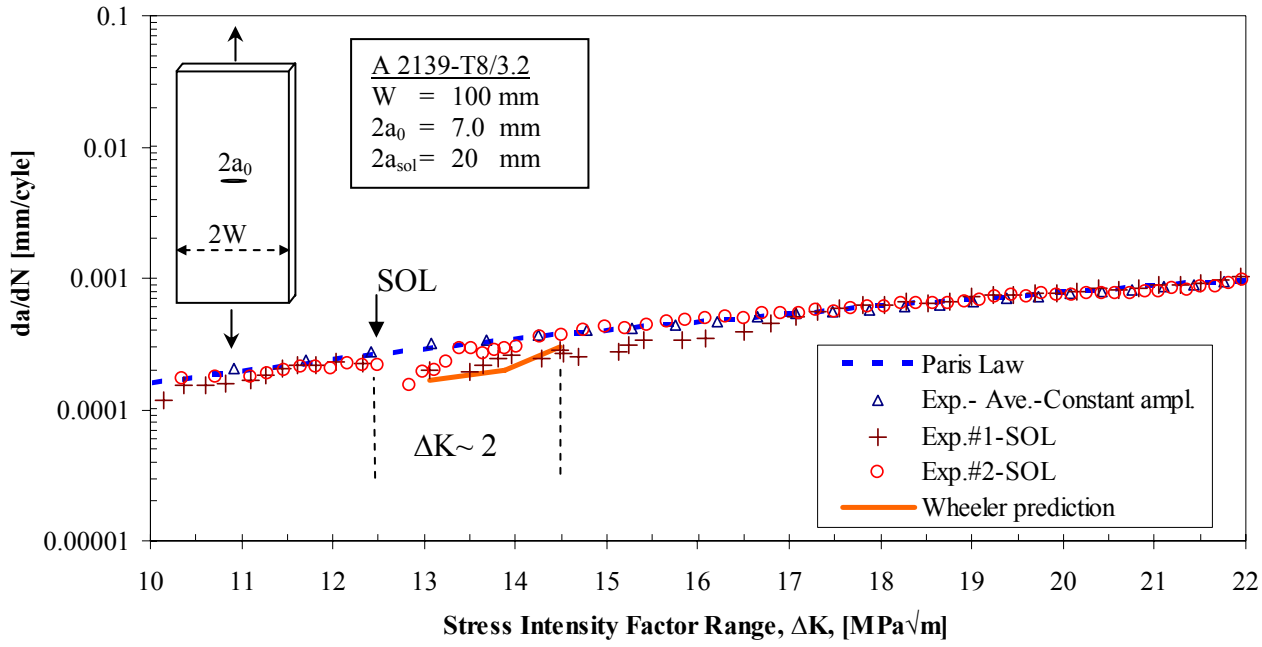

a)

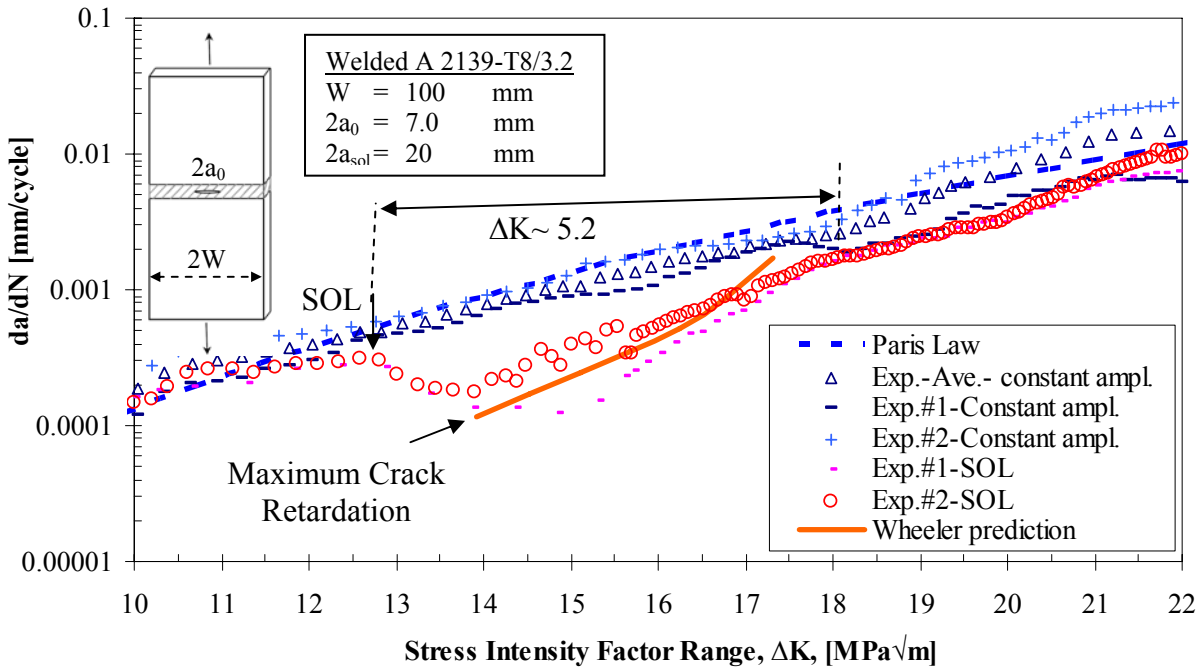

b)

Fig. 8. Crack growth rates under constant amplitude loading and SOL in a) homogeneous M(T) specimen of Al 2139-T8 and b) the laser welded M(T) specimen of Al 2139-T8